

# A detailed model of a biofilter for ammonia removal: Model parameters analysis and model validation

Guillermo Baquerizo<sup>a</sup>, Juan P. Maestre<sup>c</sup>, Takeyuki Sakuma<sup>b</sup>, Marc A. Deshusses<sup>b</sup>,  
Xavier Gamisans<sup>a</sup>, David Gabriel<sup>c,\*</sup>, Javier Lafuente<sup>c</sup>

<sup>a</sup> Department of Mining Engineering and Natural Resources, Universitat Politècnica de Catalunya, Bases de Manresa 61-73, 08240 Manresa, Spain

<sup>b</sup> Department of Chemical and Environmental Engineering, University of California, Riverside, 92521 CA, USA

<sup>c</sup> Department of Chemical Engineering, Universitat Autònoma de Barcelona, Edifici C, 08193 Bellaterra, Barcelona, Spain

Received 24 November 2004; received in revised form 16 February 2005; accepted 27 February 2005

## Abstract

A dynamic model to describe ammonia removal in a gas-phase biofilter was developed. The mathematical model is based on discretized mass balances and detailed nitrification kinetics that include inhibitory effects caused by free ammonia (FA) and free nitrous acid (FNA). The model has been able to predict experimental results for dynamic operation under different loading rates (from 3.2 to 17.2 g NH<sub>3</sub> h<sup>-1</sup> m<sup>-3</sup>). In particular the model was capable of predicting the outlet ammonia gas concentrations as well as reproducing satisfactorily the gaseous ammonia concentration profile with time under FA inhibition and under non-inhibitory conditions. A sensitivity analysis showed that pH strongly influences the results of the model.

© 2005 Elsevier B.V. All rights reserved.

**Keywords:** Biofilter; Modelling; Ammonia; Nitrification kinetics

## 1. Introduction

Ammonia is a highly odorous gas produced by organic waste treatment facilities and other industrial sources. Common air pollution control processes for polluted emissions are physical and/or chemical. However, biological treatments have become an effective and inexpensive alternative to conventional treatment systems. In particular biofiltration has been successfully applied for treating large air streams with low ammonia concentrations [1]. In biofiltration the contaminated air to be treated is passed through a packed bed where biodegradable gases or volatile compounds are absorbed into the biofilm in which diffusion and aerobic biodegradation occur simultaneously. Hence, biofiltration is a complex process that involves several physical, chemical and biological interactions.

A large number of experimental studies have demonstrated that biofiltration is an efficient biological process to remove

polluted air emissions. However, theoretical studies regarding biofilter modeling are relatively limited. Most of the work found in the literature deals with models for steady state conditions [2–4]. Nevertheless dynamic models are more suitable since operation of biofilters is often carried out under varying load conditions. Recently, Amanullah et al. [5] studied and compared different dynamic models available in the literature. Their work demonstrated that complex and realistic models are necessary to improve knowledge of biofiltration systems.

Although gas-phase biotreatment has been successfully applied to remove a large number of volatile organic compounds (VOC) and odors [6], the kinetics of biofiltration comprises biological interactions that are not well defined yet. General first- and zero-order kinetic expressions have been widely used to model the degradation process [2]. More recently, Monod kinetic models, including substrate inhibition and oxygen limitation, have been applied with satisfactory results [7,8]. As far as ammonia biotreatment is concerned many studies have established that inhibitions of bacteria affect treatment performance [1] but so far, inhibition kinetics

\* Corresponding author. Tel.: +34 935813302; fax: +34 935812013.

E-mail address: david.gabriel@uab.es (D. Gabriel).

have not been included in a biofilter model for ammonia removal.

The main objective of this work is to develop a dynamic general model to predict performance in a biofilter used to remove ammonia from air streams. The model considers most of the known phenomena that occur in biofiltration. Mathematical equations are obtained from general mass balances that take into account advection, absorption, adsorption, diffusion and biodegradation (reaction). The model includes detailed biokinetic expressions for ammonia considering all biological inhibitions occurring in the nitrification process. The model is validated using experimental results obtained from both gas phase and leachate measurements in a pilot-scale biofilter for steady state conditions. The packing material used in the experimental tests was coconut fiber obtained from a full-scale biofilter at a municipal solid waste treatment facility. Pilot-scale experiments were performed at the same operating conditions (gas contact time and watering rate) as the full-scale biofilter.

## 2. Materials and methods

### 2.1. Biofiltration unit construction and operation

Experimental data for model validation were obtained in a pilot-scale biofiltration unit that was constructed with special attention to automation (Fig. 1). The main unit, the biofilter, is a 1.1 m long, 0.1 m internal diameter transparent PVC cylinder divided in four packed bed modules where the carrier material is supported by perforated PVC plastic plates. Coconut fiber filled the four modules with a total packing height of 80 cm (20 cm each section). Gas sampling ports were lo-

cated at 20, 40 and 60 cm of packing height. Normally-closed valves located in each port allowed for automatic sampling along the bed height. The biofilter was operated in up-flow mode. The top was fitted with a spray nozzle for nutrient solution addition, while the bottom was fitted with a liquid drain. Both the liquid addition by a metering pump and leachate purge via an electrically actuated valve were controlled by a PLC.

The gas flow rate through the biofilter ( $10.46 \text{ L min}^{-1}$ ) was measured and controlled using a digital mass flow controller (DMFC) (Bronkhorst, NL). A second mass flow controller for ammonia gas ensured an accurately known concentration of ammonia at the inlet of the biofilter. Prior to mixing with ammonia, air passed through a humidification column, as it is known that humidity of less than 90–95% can result in rapid loss of biodegradation activity in the biofilter. The humidification column was made out of transparent PVC. The humidification column ensured a 99–100% relative humidity (RH) in the air entering the biofilter. A timer controlled valve added water periodically to maintain a water level in the humidification unit. The pilot unit was operated at an empty bed retention time (EBRT) of 36 s, which corresponded to the EBRT of the full-scale biofilter from which the packing material was obtained.

Continuously monitored parameters included temperature and relative humidity (Testo, Hygrotest 600 PHT), ammonia gas (Vaisala, AMT102), and data-logging of the actuation of pumps and valves. Due to some problems with the ammonia-measuring device, ammonia was ultimately measured by bubbling air samples through an acidic water trap (pH 4) in which ammonia gas was absorbed. An ammonium continuous flow analyzer was used later on for ammonia determination [9]. Additionally, a set of automated valves was used to periodi-

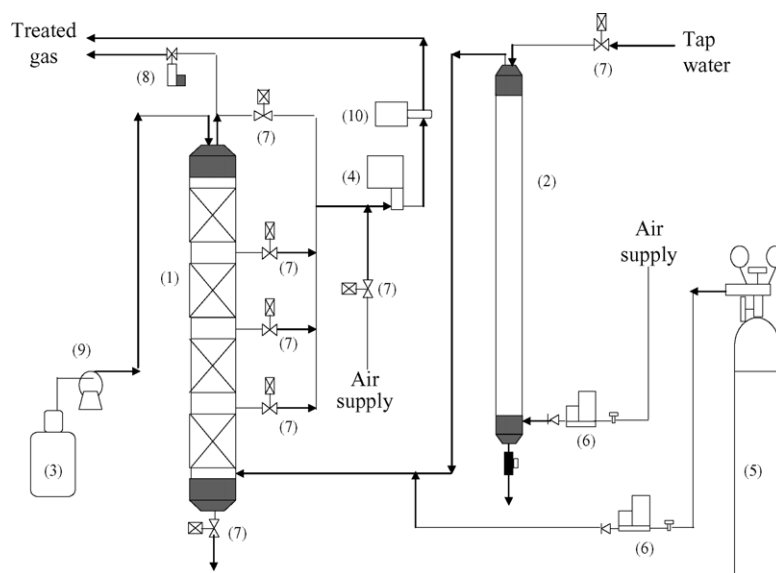


Fig. 1. Schematic representation of the biofiltration pilot-plant: (1) biofilter, (2) humidification column, (3) nutrients reservoir, (4) relative humidity and temperature sensor, (5) ammonia gas cylinder, (6) mass flow controllers, (7) normally closed valve, (8) normally opened valve, (9) pump, and (10) ammonia gas sensor.

cally pass clean air through the sensors to avoid problems of corrosion due to ammonia condensation.

A structured control system with a PLC (Siemens, S7-314C-2DP) and commercial SCADA software (Siemens, WinCC v.5.2) was used to automate the pilot-plant. The PLC acquires sensors data and executes programmed control actions such as watering, gas sampling at different bed heights and water addition to the humidification column. The SCADA program offers real-time visualization of all plant elements and continuously monitors and stores data from sensors as well as from the PLC by registering all actions taking place in the pilot-plant. WinCC controls the mass flow controllers through specialized software that allows for programming flow profiles.

## 2.2. Analytical methods and packing material characterization

During biofilter operation, leachate conductivity and pH were measured with lab probes (Crison, microCM 2100 and MicroPH 2001) prior to filtering. Leachate  $\text{Cl}^-$ ,  $\text{NO}_2^-$ ,  $\text{SO}_4^{2-}$ ,  $\text{NO}_3^-$ ,  $\text{PO}_4^{3-}$  content was determined by capillary electrophoresis in a Quanta 4000E unit (Waters) at 20 °C, 15 kV from a negative power source and indirect UV detection at 254 nm. The electrolyte used was a Waters commercial solution. Leachate  $\text{NH}_4^+$  was measured in a continuous flow analyzer [9].

Coconut fiber used as packing material in the pilot-scale biofilter was obtained from a full-scale biofilter at a municipal solid waste composting facility that mainly treats ammonia and volatile organic compounds from the foul air of the facility. Some parameters of the packing material were analyzed prior to setting up the pilot-scale biofilter (Table 1). Water and organic matter content and water holding capacity (WHC) were determined according to test methods for the examination of composting and compost [10]. Water retentivity of the packing material was determined by passing dry air through a column filled with wet coconut fiber and measuring the decrease in weight at time intervals [11]. Coconut fiber pore size and specific surface area were determined by BET adsorption isotherms of Krypton gas in a Micromeritics ASAP

2000 porosimeter. Coconut fiber density was measured in a helium pycnometer. Elementary analysis for C, N, H, P and S content of the packing material were also performed.

Except for the water content, parameters in Table 1 are inherent to the material, allowing for comparison of, e.g., pore size, specific surface area, material density, CHNSP content and organic matter content with other materials characterized in the literature [12,13]. In particular, a high specific surface area of the coconut fiber, similar to that of peat [14], is a favorable characteristic for biofiltration applications. In any case, the low pore size of the material may lead to biomass growth over the surface of the coconut fiber, thus reducing the specific surface area available for pollutant degradation.

Compared to inorganic materials tested [11] a 4–5 times lower water retentivity was found for coconut fiber. Also, the WHC at given water content may be compared. Coconut fiber at 70% water content is able to absorb up to 5.5 times its own dry weight in water, notably higher than the WHC of 2.8 g  $\text{H}_2\text{O}$  g dry material<sup>-1</sup> reported for peanut shells, a suitable packing material for biofiltration applications [12]. In any case, analyses were useful in order to gain knowledge prior to setting up the pilot-biofilter unit and to understand some operating conditions in the full-scale biofilter.

## 3. Model development

### 3.1. Microkinetics

The degradation of ammonia in the biofilter is described by a dynamic model based on mass balances combined with the detailed model of the nitrification process described by Carrera [15]. A schematic representation of the model is shown in Fig. 2.

The kinetic model considers oxidation from ammonium to nitrite and oxidation from nitrite to nitrate. Ammonium oxidation and nitrite oxidation processes were modeled considering inhibition by free ammonia (FA) and free nitrous acid (FNA). A Haldane model was used to describe substrate inhibition while ammonium oxidation inhibition by FNA and nitrite oxidation inhibition by FA were modeled as non-competitive inhibitions. Oxygen limitation is also included in the kinetic model. Since biomass growth is not considered in the model, no decay processes for ammonium- and nitrite-oxidizing biomass are considered. Therefore, the rate expressions for ammonium oxidation ( $r_A$ ) and nitrite oxidation ( $r_N$ ) are given by

$$r_A = \mu_{\max}^A \frac{S_{b,\text{O}_2}}{K_{S,\text{O}_2}^A + S_{b,\text{O}_2}} \times \frac{S_{b,\text{NH}_4}}{K_{S,\text{NH}_4}^A + S_{b,\text{NH}_4} + S_{b,\text{NH}_4}^2 / K_{I,\text{NH}_4}^A} \times \frac{K_{I,\text{NO}_2}^A}{K_{I,\text{NO}_2}^A + S_{b,\text{NO}_2}} X_A \quad (1)$$

Table 1  
Physicochemical characteristics of the coconut fiber used in this study

Parameter	Value
C (% dry weight)	47.32 ± 0.12
H (% dry weight)	5.69 ± 0.12
N (% dry weight)	0.52 ± 0.01
S (% dry weight)	Not detected
P (% dry weight)	0.23 ± 0.00
Density (g cm <sup>-3</sup> )	2.018 ± 0.006
Average pore size (Å)	109 ± 1
Specific surface area (m <sup>2</sup> g <sup>-1</sup> )	0.75 ± 0.10
Water content (%)	72.8 ± 3.2
Organic matter (% dry weight)	83.3 ± 3.1
WHC (g H <sub>2</sub> O g dry material <sup>-1</sup> )	5.5 ± 0.6
Water retentivity (% day <sup>-1</sup> )	-31 ± 7

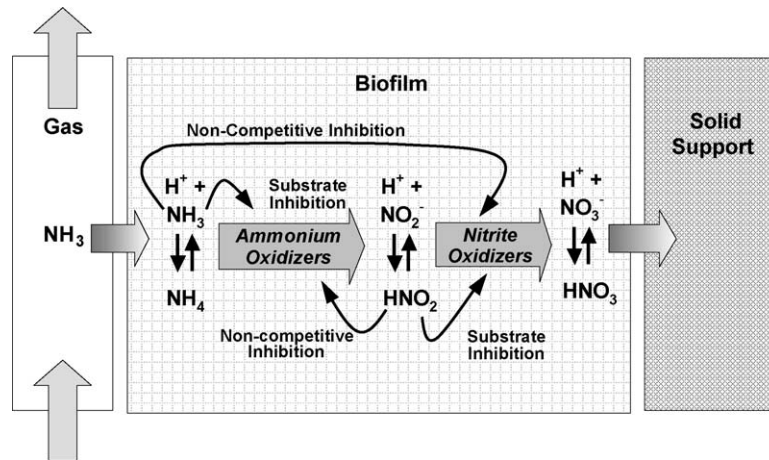


Fig. 2. Schematic representation of the nitrification process including substrate and non-competitive inhibitions.

$$r_N = \mu_{\max}^N \frac{S_{b,O_2}}{K_{S,O_2}^N + S_{b,O_2}} \times \frac{S_{b,NO_2}}{K_{S,NO_2}^N + S_{b,NO_2} + S_{b,NO_2}^2 / K_{I,NO_2}^N} \times \frac{K_{I,NH_4}^N}{K_{I,NH_4}^N + S_{b,NH_4}} X_N \quad (2)$$

where  $S_{b,NH_4}$ ,  $S_{b,NO_2}$  and  $S_{b,O_2}$  are the biofilm concentration of ammonium, nitrite and oxygen, respectively ( $\text{g m}^{-3}$ ),  $X_A$  is the ammonia-oxidizing biomass ( $\text{g COD m}^{-3}$ ), and  $X_N$  is the nitrite-oxidizing biomass ( $\text{g COD m}^{-3}$ ). The kinetic parameters and stoichiometric coefficients used for model validation are shown in Table 2. The same parameter values optimized by Carrera [15] for a nitrifying activated sludge pilot-plant were used herein for model simulations.

Inhibition coefficients ( $K_I$ ) in ammonium oxidation and nitrite oxidation are expressed in ammonium and nitrite con-

centration units although they are pH-dependent in these units. Coefficients are only constants if they are expressed as FA and FNA concentrations. Units are transformed according to ammonia–ammonium and nitrite–nitrous acid equilibriums, respectively:

$$K_{I,NH_4} = \frac{14}{17} (K_{A,FA} \times 10^{\text{pH}})^{-1} K_{I,FA} \quad (3)$$

$$K_{I,NO_2} = \frac{14}{47} (K_{A,FNA} \times 10^{\text{pH}}) K_{I,FNA} \quad (4)$$

where  $K_{I,NH_4}$  is any inhibition coefficient by FA in  $\text{mg N-NH}_4^+ \text{L}^{-1}$  and  $K_{I,NO_2}$  is any inhibition coefficient by FNA in  $\text{mg N-NO}_2^- \text{L}^{-1}$ .  $K_{A,FA}$  is the ionization constant of the ammonia–ammonium equilibrium and  $K_{A,FNA}$  the ionization constant of the nitrous acid–nitrite equilibrium.

Table 2  
Kinetic and stoichiometric parameters of the nitrification model

Parameter	Symbol	Units	Value
<b>Kinetic parameters</b>			
<b>Ammonium-oxidizing biomass</b>			
Maximum growth rate	$\mu_{\max}^A$	$\text{day}^{-1}$	0.82
Half-saturation coefficient for oxygen	$K_{S,O_2}^A$	$\text{mg O}_2 \text{L}^{-1}$	0.5
Half-saturation coefficient for ammonium	$K_{S,NH_4}^A$	$\text{mg N-NH}_4^+ \text{L}^{-1}$	4.8
Inhibition coefficient for FA	$K_{I,FA}^A$	$\text{mg FA L}^{-1}$	$116 \pm 24$
Inhibition coefficient for FNA	$K_{I,FNA}^A$	$\text{mg FNA L}^{-1}$	$0.59 \pm 0.04$
<b>Nitrite-oxidizing biomass</b>			
Maximum growth rate	$\mu_{\max}^N$	$\text{day}^{-1}$	2.0
Half-saturation coefficient for oxygen	$K_{S,O_2}^N$	$\text{mg O}_2 \text{L}^{-1}$	0.5
Half-saturation coefficient for nitrite	$K_{S,NO_2}^N$	$\text{mg N-NO}_2^- \text{L}^{-1}$	3.5
Inhibition coefficient for FA	$K_{I,FA}^N$	$\text{mg FA L}^{-1}$	0.52
Inhibition coefficient for FNA	$K_{I,FNA}^N$	$\text{mg FNA L}^{-1}$	$0.065 \pm 0.009$
<b>Stoichiometric parameters</b>			
Yield coefficient for ammonia-oxidizing biomass	$Y_A$	$\text{mg COD mg N}^{-1}$	0.27
Yield coefficient for nitrite-oxidizing biomass	$Y_N$	$\text{mg COD mg N}^{-1}$	0.22

### 3.2. Mass balances

A mathematical model was developed for the biofilter based on mass balance equations. Four phases were considered in the system: gas, liquid, biofilm, and solid. The liquid phase is included due to periodic watering. Although coconut fiber has little porosity, an equation for the adsorption process into the packing material was included because of the aim of developing a general model of biofiltration.

Mass balance equations were described on the basis of the following assumptions:

- (1) The flow pattern of the bulk gas is plug flow.
- (2) A plug flow pattern is considered for liquid flow when water is added.
- (3) Consistent with the film theory, gas–liquid interface is always in equilibrium as dictated by Henry’s law. Additionally, no resistance in the liquid–biofilm interface is assumed since biofilm is formed mainly by liquid. Liquid–biofilm interface concentrations are considered identical.
- (4) A single individual gas mass-transfer coefficient ( $k_g$ ) is used for calculating the mass flux at the gas–liquid interface for all nitrogen species since their diffusion coefficients have similar values.
- (5) The diffusion in the biofilm is described by Fick’s law.
- (6) Biofilm is formed on the external surface of the packing material. Biomass does not grow in the pores of particles and therefore reactions occur only in the biofilm phase.
- (7) Planar geometry and perpendicular diffusion in the biofilm–gas interface can be used to derive model equations.
- (8) During watering periods, the biofilm surface is uniformly wetted by the liquid flow.
- (9) Physical properties of the biofilm (Henry coefficients, diffusion coefficients, acid–base equilibrium) are assumed the same as in water [2,7].
- (10) There is no accumulation of biomass in the filter bed, even though different biomass concentrations are considered along the bed height. Biomass properties (thickness, specific surface area and kinetic coefficients) are uniform along the bed, and constant under different operating conditions.

In the gas phase, ammonia, nitrous acid, nitric acid and oxygen are the sole state variables considered. The variables considered in the liquid, biofilm and solid phases are total ammonia as the sum of free ammonia and ammonium, total nitrite as the sum of free nitrous acid and nitrite, total nitrate as the sum of nitric acid and nitrate, and oxygen.

The nomenclature used to distinguish single ( $S$ ) and total ( $C$ ) compounds is shown in Eqs. (5)–(7):

$$C_{\text{phase,NTNH}} = S_{\text{phase,NH}_4} + S_{\text{phase,NH}_3} \quad (5)$$

$$C_{\text{phase,NTNO}_2} = S_{\text{phase,HNO}_2} + S_{\text{phase,NO}_2} \quad (6)$$

$$C_{\text{phase,NTNO}_3} = S_{\text{phase,HNO}_3} + S_{\text{phase,NO}_3} \quad (7)$$

where the subscripts ‘phase’ is ‘g’ for the gas phase, ‘l’ for the liquid phase, ‘b’ for the biofilm phase, and ‘s’ for the solid phase; the subscript NTNH means total ammonia, NTNO<sub>2</sub> means total nitrite, and NTNO<sub>3</sub> means total nitrate.

Equilibrium expressions for ammonia–ammonium, nitrite–nitrous acid and nitrate–nitric acid and an experimental pH profile were used to calculate the concentration of each single compound from total ammonia, total nitrite and total nitrate. These assumptions result in the following set of equations:

#### 3.2.1. Mass balance for the bulk gas phase:

$$\frac{\partial S_{g,j}}{\partial t} = -v_z \frac{\partial S_{g,j}}{\partial z} - \frac{a}{\varepsilon} N_{gl}, \quad j = \text{NH}_3, \text{HNO}_2, \text{HNO}_3, \text{O}_2 \quad (8)$$

$$\text{at } z = 0, \quad S_{g,j} = S_{g,j}^{\text{in}} \quad (9)$$

where  $v_z$  is the interstitial gas velocity ( $\text{m h}^{-1}$ ),  $S_{g,j}^{\text{in}}$  the inlet gas concentration ( $\text{g m}^{-3}$ ) for component  $j$ ,  $z$  the position along the biofilter height (m),  $a$  the specific surface area (biofilm surface area per unit volume of biofilter bed,  $\text{m}^2 \text{m}^{-3}$ ),  $\varepsilon$  the porosity of the filter bed (non-dimensional). A true volume fraction occupied by the gas ( $\varepsilon$ ) is calculated subtracting the volume fraction occupied by the biomass and the volume fraction occupied by the liquid ( $h_c$ ), the latter only during watering periods, from clean bed void fraction ( $\varepsilon^*$ ).  $N_{gl}$  is the mass flux from the gas phase to the liquid phase ( $\text{g m}^{-2} \text{h}^{-1}$ ) given by

$$N_{gl} = k_g(S_{g,j} - S_{g,i,j}) = k_g(S_{g,j} - S_{l,j}H) \quad (10)$$

where  $k_g$  is the individual gas mass-transfer coefficient ( $\text{m h}^{-1}$ ),  $S_{g,i,j}$  the gas concentration at the gas–liquid interface for component  $j$  ( $\text{g m}^{-3}$ ),  $S_{l,j}$  the liquid concentration for component  $j$  ( $\text{g m}^{-3}$ ), and  $H$  is the gas–liquid distribution coefficient given by Henry’s law. Since only ammonia, nitrous and nitric acid are present in the gas phase, concentrations of these compounds both in the liquid phase and in the gas phase were used for calculating the mass flux between the gas and the liquid phase.

#### 3.2.2. Mass balance for the liquid phase:

$$\frac{\partial C_{l,j}}{\partial t} = v_l \frac{\partial C_{l,i}}{\partial z} + \frac{a}{h_c} N_{gl} - \frac{a}{h_c} N_{lb}, \quad j = \text{NTNH}, \text{NTNO}_2, \text{NTNO}_3, \text{O}_2 \quad (11)$$

$$\text{at } z = L, \quad C_{l,j} = C_{l,j}^{\text{in}} \quad (12)$$

where  $v_l$  the interstitial liquid velocity ( $\text{m h}^{-1}$ ),  $h_c$  the dynamic hold-up (non-dimensional),  $N_{lb}$  the mass flux from the liquid phase to the biofilm phase ( $\text{g m}^{-2} \text{h}^{-1}$ ),  $L$  the biofilter

packing height (m), and  $C_{1,j}^{\text{in}}$  the inlet liquid concentration for component  $j$  ( $\text{g m}^{-3}$ ). Note that  $N_{\text{lb}}$  is given by Fick's law:

$$N_{\text{lb}} = -D_j \left( \frac{\partial C_{b,j}}{\partial x} \right) \Big|_{x=0} \quad (13)$$

where  $D_j$  is the diffusion coefficient for component  $j$  ( $\text{m}^2 \text{h}^{-1}$ ),  $C_{b,j}$  the concentration in biofilm phase for component  $j$  ( $\text{g m}^{-3}$ ), and  $x$  the position in the biofilm (m).

### 3.2.3. Mass balance for the biofilm:

$$\frac{\partial C_{b,j}}{\partial t} = D_i \frac{\partial^2 C_{b,j}}{\partial x^2} + r, \quad (14)$$

$$j = \text{NTNH}, \text{NTNO}_2, \text{NTNO}_3, \text{O}_2$$

$$\text{at } x = 0, \quad C_{b,j} = C_{1,j} \quad (15)$$

$$\text{at } x = \delta, \quad -D_j \left( \frac{\partial C_{b,j}}{\partial x} \right) \Big|_{x=\delta} = -D_j \left( \frac{\partial C_{s,j}}{\partial x} \right) \Big|_{x=\delta} \quad (16)$$

where  $r$  is the substrate utilization rate ( $\text{g m}^{-3} \text{h}^{-1}$ ),  $\delta$  the biofilm thickness (m), and  $C_{s,j}$  the concentration in solid phase for component  $j$  ( $\text{g m}^{-3}$ ).

### 3.2.4. Mass balance for the solid phase:

$$\frac{\partial C_{s,j}}{\partial t} = \frac{a}{1 - \varepsilon - h_c - h_b} N_{\text{bs}}, \quad (17)$$

$$j = \text{NTNH}, \text{NTNO}_2, \text{NTNO}_3, \text{O}_2$$

where  $h_b$  is the volume fraction occupied by the biofilm (non-dimensional), and  $N_{\text{bs}}$  the mass flux from the biofilm phase to the solid phase given by

$$N_{\text{bs}} = -D_j \left( \frac{\partial C_{b,j}}{\partial x} \right) \Big|_{x=\delta} \quad (18)$$

The set of partial differential equations was discretized in space along the bed height and biofilm thickness. Twelve points were used along the bed length, and four points were used along the biofilm thickness. The resulting set of ordinary differential equations was solved using MATLAB in a home-made modeling environment. A low, variable order non-stiff integration method based on the numerical differentiation formulas (NDFs) was used to solve mathematical equations after testing different integration methods provided by MATLAB. Initial conditions for all state variables were set equal to zero.

## 4. Results and discussion

### 4.1. Performance of coconut fiber in biofiltration of ammonia

An experiment was undertaken in the pilot-scale biofilter once the coconut fiber withdrawn from the full-scale biofilter was characterized. No inoculation was needed since the full-scale biofilter had been running for more than 2 years at an average ammonia inlet concentration of 40 ppm<sub>v</sub>. Still a 15-day acclimation period at 45 ppm<sub>v</sub> was allowed after initial start of the pilot unit. After that, four-step increases in the ammonia inlet concentration were performed for a minimum of 3 days each (0–45, 45–123.2, 123.2–244.2, 244.2–187.4 ppm<sub>v</sub>) (Fig. 3) to reach new steady states. Room temperature ( $22 \pm 2^\circ \text{C}$ ) was maintained during the operation. Since the EBRT was 36 s, the inlet loading ranged from 3.2 to 17.2  $\text{g NH}_3 \text{h}^{-1} \text{m}^{-3}$ . Watering was performed once per day for a period of 6 s at a water flow rate of 0.270  $\text{L day}^{-1}$ . Elimination capacities and removal efficiencies reached at the end of each feeding period were 3.2  $\text{g NH}_3 \text{h}^{-1} \text{m}^{-3}$  and 100% for the 45 ppm<sub>v</sub> feeding period, 8.6  $\text{g NH}_3 \text{h}^{-1} \text{m}^{-3}$  and 98.7% for the 123.2 ppm<sub>v</sub> feeding period, 9.5  $\text{g NH}_3 \text{h}^{-1} \text{m}^{-3}$  and 55.0% for the 244.2 ppm<sub>v</sub> feeding period, and 11.4  $\text{g NH}_3 \text{h}^{-1} \text{m}^{-3}$  and 86.2% for the

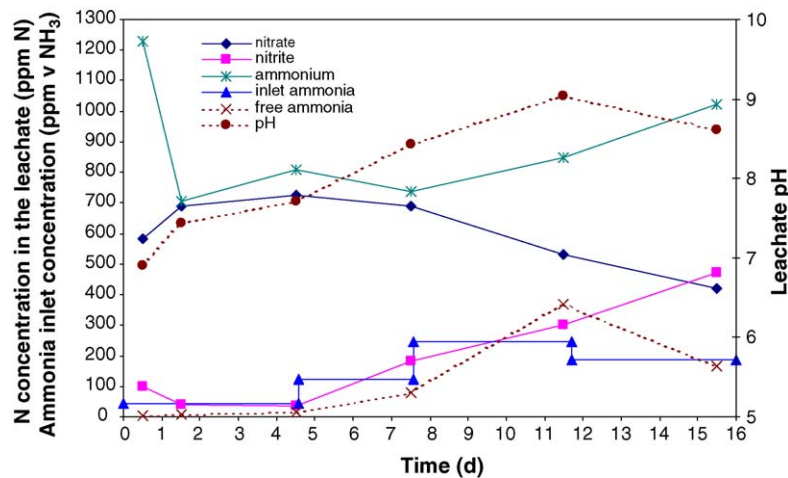


Fig. 3. Experimental evolution for nitrite, nitrate, ammonium and pH in the leachate and programmed profile of inlet  $\text{NH}_3$ .

187.4 ppm<sub>v</sub> feeding period. Monitoring of leachate and ammonia gas concentration was performed at the end of each period and all water collected for each period was kept for leachate analysis. Gas samples were taken automatically from the outlet air stream, as well as from the three sampling ports along the height of the biofilter. Inlet ammonia concentration was measured by manually sampling the inlet air stream. Inlet ammonia concentrations measured were in close agreement with those expected from mass flow controller calculations.

Fig. 3 shows that nitrite and free ammonia began to accumulate after the 123.2 ppm<sub>v</sub> feeding period and nitrate concentration decreased concurrently. During the 244.2 ppm<sub>v</sub> feeding period the same trend was observed, which was related to inhibitory conditions of the nitrification process. Once the ammonia load was decreased during the 187.4 ppm<sub>v</sub> feeding period, no reverse trend in the nitrate and nitrite concentrations were observed, indicating that inhibitory conditions remained thereafter during the 187.4 ppm<sub>v</sub> feeding period.

Based on the inhibition constants used in the kinetic model (Table 2) and the pH measured in the leachate, inhibition was determined to be caused by the accumulation of free ammonia (FA) rather than free nitrous acid (FNA), even though these calculations were based on the concentrations measured in the leachate, instead of those in the biofilm, which might be notably higher. The ammonium oxidation rates calculated in each period showed that ammonia to nitrite conversion was mostly inhibited after the 244.2 ppm<sub>v</sub> feeding period. Instead, the nitrification rate showed a decrease after the 123.2 ppm<sub>v</sub> feeding period, which indicated that the conversion of nitrite to nitrate is more severely affected by ammonia inhibition than the conversion of ammonia to nitrite.

#### 4.2. Modeling of the experimental data

Model parameters were set from both experimental data and from the literature. The values of the kinetic and stoichiometric parameters used in the simulations are shown in Table 2. Also, well-accepted values for distribution coefficients were used, while diffusion coefficients and biofilm

thickness were adapted from reliable literature sources (Table 3).

The individual gas mass-transfer coefficient for nitrogen compounds ( $k_g$ ) was the main physicochemical parameter optimized by simulation. In addition to this, biomass concentrations in each module were optimized assuming a decrease in the direction of flow, consistent with the observations of several investigators. As expected, ammonia gas concentrations measured along the bed height (Fig. 4a and b) indicated a trend for the elimination capacity to decrease in the direction of flow, but a sharper decrease in the ammonia concentration observed in the first module indicated that a higher concentration of nitrifying biomass had developed in the module closest to the inlet of the biofilter.

Ammonia-oxidizing biomass and nitrite-oxidizing biomass densities in the biofilm were optimized following the ratio given by Carrera [15] in which the concentration of nitrite-oxidizing biomass corresponds to one third of ammonia-oxidizing biomass. A two times higher biomass density for both biomasses was needed in the lower module compared to the other upper three modules to properly describe the ammonia gas profiles at both low (Fig. 4a) and high ammonia inlet loads (Fig. 4b). The sharp-slope changes in Fig. 4 are due to the non-uniform biomass distribution along the bed height. Experimental data shown in Fig. 4(a) and (b) were obtained at the end of each feeding period, once a quasi-steady state was reached. In addition, since proton concentration was not included in the model as a state variable, a pH profile was programmed to emulate the experimental pH measured in the leachate.

The four sequential feeding periods were simulated under dynamic conditions. Fig. 5 shows the experimental data and model predicted profiles for outlet ammonia concentration considering models with and without inhibition by FA and FNA. Intermittent watering operation leads to a decrease of the outlet gas concentration due to a major absorption capacity in the water phase, thus reducing the gas concentration at the outlet as observed in the simulated profiles in Fig. 5. The model predictions conducted with inhibition kinetics are in good agreement with experimental results indicating that

Table 3  
Values of physical parameters used in the model

Parameter	Value	Reference
Diffusion of total ammonia, $D_{NTNH}$ (m <sup>2</sup> h <sup>-1</sup> )	$4.97 \times 10^{-6}$	[16]
Diffusion of total nitrite, $D_{NTNO_2}$ (m <sup>2</sup> h <sup>-1</sup> )	$4.43 \times 10^{-6}$	[16]
Diffusion of total nitrate, $D_{NTNO_3}$ (m <sup>2</sup> h <sup>-1</sup> )	$4.43 \times 10^{-6}$	[16]
Diffusion of oxygen, $D_O$ (m <sup>2</sup> h <sup>-1</sup> )	$1.96 \times 10^{-6}$	[17]
Distribution coefficient for ammonia, $H_{NH_3}$ (-)	$6.7 \times 10^{-4}$	[18]
Distribution coefficient for nitrous acid, $H_{HNO_2}$ (-)	$8.2 \times 10^{-4}$	[19]
Distribution coefficient for nitric acid, $H_{HNO_3}$ (-)	$1.9 \times 10^{-7}$	[20]
Distribution coefficient for oxygen, $H_O$ (-)	34.4	[17]
Individual gas mass-transfer coefficient, $k_g$ (m h <sup>-1</sup> )	3.5	Adjusted by simulation
Porosity of the clean filter bed, $\epsilon^*$ (-)	0.7	Experimental determination
Dynamic hold-up, $h_c$ (-)	0.1	Adjusted by simulation
Specific surface area, $a$ (m <sup>2</sup> m <sup>-3</sup> )	360	Experimental determination and adapted from [12]
Biofilm thickness, $\delta$ (μm)	100	[7]

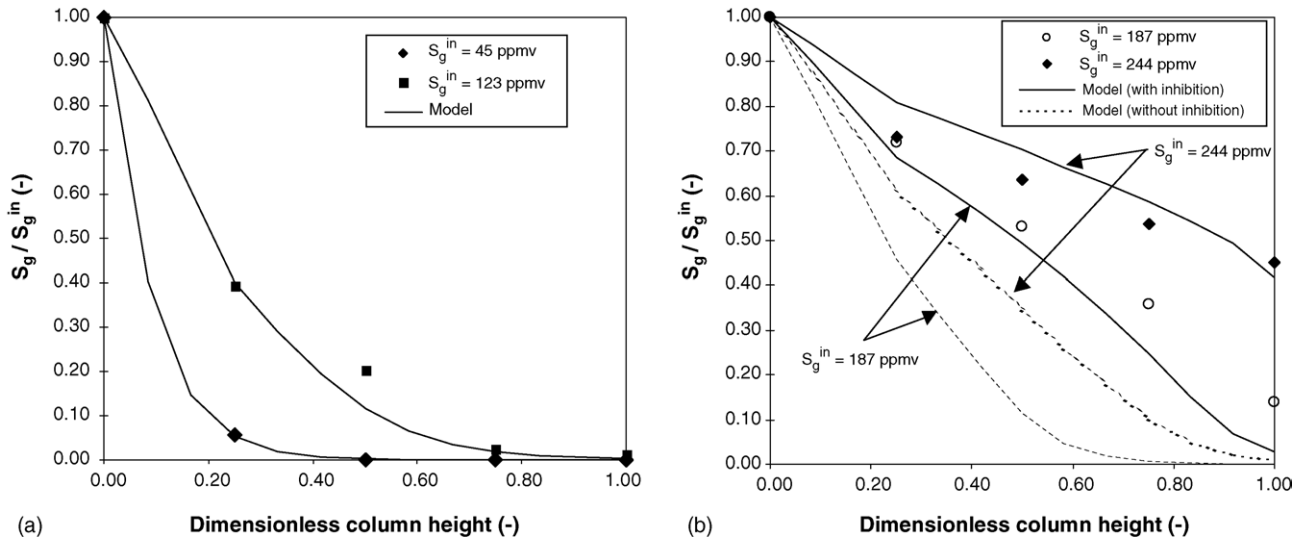


Fig. 4. Gas concentration profiles along the biofilter bed for: (a) low ammonia inlet concentration and (b) high ammonia inlet concentration.

including inhibition is necessary to reproduce the outlet concentration under higher ammonia load periods and that inhibition effects are adequately integrated in the model.

In addition to this, experimental and simulated profiles plotted as a function of the biofilter dimensionless height (Fig. 4(a) and (b)) showed that the model is capable of accurately predicting the behavior of the reactor along the bed height for both low and high inlet concentrations, the latter under inhibitory operating conditions. It is worth mentioning that the ammonia concentration along the bed height is not well predicted for the 187.4 ppm<sub>v</sub> feeding period, i.e., right after the highest concentration of ammonia tested (Fig. 4b). The model predicted lower concentrations with and without inhibition than experimentally observed. This is most probably due to the difficulty of biomass to recover its biodegradation activity once inhibitory conditions have affected the cells because of the lingering effects of inhibition. Lingering effects are not taken into account in the model in its present form, thus only inhibitory effects due to the 187.4 ppm<sub>v</sub> feeding period without accounting for a previous inhibition period are predicted by the model. Normally, more than a week might be necessary to recover biomass degradation capacity after an inhibition episode.

#### 4.3. Sensitivity analysis of model parameters

A sensitivity analysis was performed for the kinetic, stoichiometric and physicochemical parameters shown in Tables 2 and 3 except for distribution coefficients and Henry constants, which were not included, as they are true constants. Additionally, pH was included in the sensitivity analysis as an operational parameter because of its influence on equilibrium and inhibition constants. Simulations were performed under a constant feed of 244.2 ppm<sub>v</sub> of ammonia gas concentration until the steady state was reached. The elimination capacity of the biofilter and the outlet concentration from the lower module of the reactor were chosen as state variables. Sensitivity was assessed by increasing and decreasing 10% the values of the parameters in Tables 2 and 3 (the default parameters), and comparing the relative change of the state variables to a relative change of the value of the parameter according to the following expression:

$$\text{sensitivity} = \frac{\Delta V / V_d}{|\Delta P / P_d|} \quad (19)$$

where  $\Delta V$  means the difference between the simulated variable under the new conditions and the value of the variable in

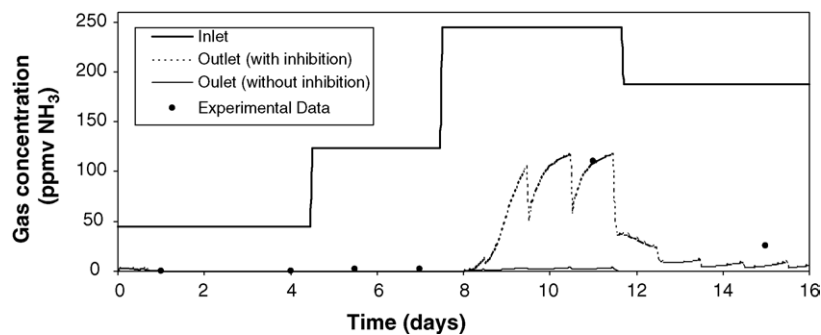


Fig. 5. Dynamic simulation of ammonia outlet concentration predicted by the model (with and without inhibition) compared to experimental data.

Table 4  
Sensitivity results for outlet concentration from module 1 ( $C_{out,1}$ ) and elimination capacity of the biofilter (EC) for selected parameters of the model

Parameter	$\Delta$ (%)	Sensitivity, $C_{out,1}$	Sensitivity, EC
$a$	+10	-0.33	1.21
	-10	0.32	-1.10
$\delta$	+10	-0.30	1.12
	-10	0.31	-1.06
$h_c$	+10	0.00	0.00
	-10	0.00	0.01
$k_g$	+10	-0.08	0.29
	-10	0.11	-0.44
$\mu_{max}^A X_A$	+10	-0.27	0.45
	-10	0.27	-0.44
$K_{I,FA}^A$	+10	-0.20	0.64
	-10	0.21	-0.68
$K_{I,FNA}^A$	+10	-0.01	0.02
	-10	0.01	-0.03
$Y_A$	+10	0.28	-0.98
	-10	-0.35	1.30
pH	+10	0.03	-0.86
	-10	-3.98	6.93

the default conditions ( $V_d$ ). Similarly,  $\Delta P$  means the difference between the value of the parameter at the  $\pm 10\%$  change and the value of the default parameter ( $P_d$ ).

Table 4 shows that physicochemical parameters have a notable impact. This is consistent with other studies reported in the literature [17], even though most studies found in the literature were performed using either first- or zero-order kinetics. The minor influence of  $k_g$  might be explained by the high value used as default parameter, which led to a biologically limited system, rather than a gas-transfer limited one. Related to this, the large  $k_g$  to  $h_c$  ratio explains the negligible influence of  $h_c$  during watering periods, indicating that the mass flux from the gas to the liquid and the mass flux from the liquid to the biofilm are not limited by the amount of water retained in the bioreactor.

Regarding the kinetic and stoichiometric parameters, no influence was found for those parameters related to nitrite-oxidizing biomass ( $\mu_{max}^N X_N$ ,  $Y_N$ ) since ammonia gas concentration is not affected by the nitrite oxidation rate if enough nitrite is present. Similarly,  $K_{I,FNA}^A$  has a minor influence since biological processes were only affected by FA inhibition under the conditions simulated. It is worth noting that  $\mu_{max}^A$  and  $X_A$  were lumped in a single parameter due to the inability to assign separate values to each parameter, at this time in the study. The large influence of  $Y_A$  suggests that the use of a sole parameter  $\mu' = \mu X/Y$  would be preferable in terms of identification of model parameters, as is usually used by other authors in the literature.

Finally, the strong influence of the pH in the results of the sensitivity analysis must be emphasized. This was expected because the pH governs equilibria among all nitrogen species, which in turn affect the distribution of the compounds. This

directly affects the extent of the inhibition constants by FA and FNA, and ultimately affects the biological conversion rates of the nitrification process. In addition, the parameters presented above, may be significantly affected by the pH, which was based on selected experimental pH value, rather than simulated. Accurate pH determinations, or better expanding the model to include  $H^+$ -ion balances are warranted in order to ensure good results.

## 5. Conclusions

The mathematical model presented herein includes most of the phenomena occurring in a biofilter. The model was able to describe the ammonia removal in a gas-phase bioreactor by predicting removal profiles and ammonia outlet concentrations under inhibitory and non-inhibitory operating conditions. Of particular importance was the inclusion of detailed nitrification kinetics that take into account inhibition of free ammonia and free nitrous acid. Thus, the model is able to predict ammonia shock-loadings and bioreactor behavior under inhibitory conditions. Several improvements are being explored. These include a description of the lag phase for biomass recovery after an inhibition period. Most important, the addition of proton concentrations as a state variable is warranted and would enhance model predictions due to the strong influence of the pH in the inhibition kinetics and in the equilibria of the species involved.

## Acknowledgements

This work was supported by the Spanish CICYT project PPQ2003-02482. The Department of Chemical Engineering at UAB is a unit of Biochemical Engineering of the Centre de Referència en Biotecnologia de Catalunya (CeRBA), Generalitat de Catalunya.

## References

- [1] N.-J. Kim, Y. Sugano, M. Hirai, M. Shoda, Removal of a high load of ammonia gas by a marine bacterium, *Vibrio alginolyticus*, J. Biosci. Bioeng. 90 (2000) 410–415.
- [2] S.P.P. Ottengraf, H.C. Van der Oever, Kinetics of organic compound removal from waste gases with a biological filter, Biotechnol. Bioeng. 25 (1983) 3089–3102.
- [3] B.C. Baltzis, S.M. Wojdyla, S.M. Zarook, Modeling biofiltration of VOC mixtures under steady-state conditions, J. Environ. Eng. ASCE 123 (1997) 599–605.
- [4] S.M. Zarook, A.A. Shaikh, Analysis and comparison of biofilter models, Chem. Eng. J. 65 (1997) 55–61.
- [5] Md. Amanullah, S. Farooq, S. Viswanathan, Modeling and simulation of a biofilter, Ind. Eng. Chem. Res. 38 (1999) 2765–2774.
- [6] J.S. Devinny, M.A. Deshusses, T.S. Webster, Biofiltration for Air Pollution Control, Lewis Publishers, New York, 1999.
- [7] M.A. Deshusses, G. Hamer, I. Dunn, Behavior of biofilters for waste air biotreatment. 1. Dynamic model development, Environ. Sci. Technol. 29 (1995) 1048–1058.

- [8] S.M. Zarook, A.A. Shaikh, Z. Ansar, Development, experimental validation and dynamic analysis of a general transient biofilter model, *Chem. Eng. Sci.* 52 (1997), 759–753.
- [9] J.A. Baeza, D. Gabriel, J. Lafuente, An expert supervisory system for a pilot WWTP, *Environ. Model. Softw.* 14 (1999) 383–390.
- [10] U.S. Composting Council, in: P.B. Leege, W.H. Thompson (Eds.), *Test Methods for the Examination of Composting and Compost*, USCC, Bethesda, MD, US, 1995.
- [11] M. Hirai, M. Kamamoto, M. Yani, M. Shoda, Comparison of the biological H<sub>2</sub>S removal characteristics among four inorganic packing materials, *J. Biosci. Bioeng.* 91 (2001) 396–402.
- [12] E. Ramirez-Lopez, J. Corona-Hernandez, L. Dendooven, P. Rangel, F. Thalasso, Characterization of five agricultural by-products as potential biofilters carriers, *Bioresour. Technol.* 88 (2003) 259–263.
- [13] H.L. Bohn, Biofilter media, in: *Proceedings of the 89th Annual Meeting and Exhibition of Air and Waste Management Association*, Nashville, US, 1996.
- [14] M. Zilli, B. Fabiano, A. Ferraiolo, A. Converti, Macro-kinetic investigation on phenol uptake from air by biofiltration—influence of superficial gas-flow rate and inlet pollution concentration, *Biotechnol. Bioeng.* 49 (1996) 391–398.
- [15] J. Carrera, Biological nutrient removal from high-strength wastewater: analysis of process parameters and design of a full-scale wastewater treatment plant, Ph.D. Thesis, Universitat Autònoma de Barcelona Ed., 2000 (in Spanish).
- [16] H. Satoh, H. Ono, B. Rulin, J. Kamo, S. Okabe, K.-I. Fukushi, Macroscale and microscale analyses of nitrification and denitrification in biofilms attached on membrane aerated biofilm reactors, *Water Res.* 38 (2004) 1633–1641.
- [17] Z. Shareefdeen, B.C. Baltzis, Y.-S. Oh, R. Bartha, Biofiltration of methanol vapor, *Biotechnol. Bioeng.* 41 (1993) 512–524.
- [18] S.L. Clegg, P. Brimblecombe, Solubility of ammonia in pure aqueous and multicomponent solutions, *J. Phys. Chem.* 93 (1989) 7237–7238.
- [19] K.H. Becker, J. Kleffmann, R. Kurtenbach, P. Wiesen, Solubility of nitrous acid (HONO) in sulfuric acid solutions, *J. Phys. Chem.* 100 (1996) 14984–14990.
- [20] S.E. Schwartz, W.H. White, Solubility equilibria of the nitrogen oxides and oxyacids in dilute aqueous solutions, in: J.R. Pfaflin, E.N. Ziegler (Eds.), *Advances in Environmental Science and Engineering*, vol. 4, Gordon and Breach Science Publishers, New York, 1981, pp. 1–45.